Geophys. J. Int. (2007) **170,** 1076–1088 doi: 10.1111/j.1365-246X.2007.03531.x

Run-up from impact tsunami

D. G. Korycansky[1] and Patrick J. Lynett[2]

[1]*Department Earth and Planetary Sciences, University of California, Santa Cruz,* CA 95064*, USA. E-mail: kory@pmc.ucsc.edu*
[2]*Coastal and Ocean Engineering Division, Department of Civil Engineering, Texas A&M University, College Station,* TX 77843*, USA*

Accepted 2007 June 21. Received 2007 June 18; in original form 2007 January 10

SUMMARY

We report on calculations of the on-shore run-up of waves that might be generated by the impact of subkilometre asteroids into the deep ocean. The calculations were done with the COULWAVE code, which models the propagation and shore-interaction of non-linear moderate- to long-wavelength waves ($kh < \pi$) using the extended Boussinesq approximation. We carried out run-up calculations for several different situations: (1) laboratory-scale monochromatic wave trains onto simple slopes; (2) 10–100 m monochromatic wave trains onto simple slopes; (3) 10–100 m monochromatic wave trains onto a compound slope representing a typical bathymetric profile of the Pacific coast of North America; (4) time-variable scaled trains generated by the collapse of an impact cavity in deep water onto simple slopes and (5) full-amplitude trains onto the Pacific coast profile. For the last case, we also investigated the effects of bottom friction on the run-up. For all cases, we compare our results with the so-called 'Irribaren scaling': The relative run-up $R/H_0 = \xi = s(H_0/L_0)^{-1/2}$, where the run-up is R, H_0 is the deep-water waveheight, L_0 is the deep-water wavelength, s is the slope and ξ is a dimensionless quantity known as the Irribaren number. Our results suggest that Irribaren scaling breaks down for shallow slopes $s \leq 0.01$ when $\xi < 0.1 - 0.2$, below which R/H_0 is approximately constant. This regime corresponds to steep waves and very shallow slopes, which are the most relevant for impact tsunami, but also the most difficult to access experimentally.

Key words: hydrodynamics, impact tsunami, run-up, wave propagation.

1 INTRODUCTION

Tsunami generated by the impacts of asteroids or comets are widely recognized as a potential hazard (Chapman & Morrison 1994; Hills *et al.* 1994; Atkinson *et al.* 2000; Ward & Asphaug 2000; Chesley & Ward 2006). The global reach of ocean waves generated in an impact could enhance the effect of impacts whose scope would otherwise be of regional importance only. The hazard is compounded by the concentration of the world's population and economic activity near ocean shorelines. It is important to examine the potential consequences of a sizeable oceanic impact. Direct observational experience with impact tsunami is lacking; typical periods fall between the familiar ranges of storm waves on the one hand, and earthquake tsunami, on the other. However, large-amplitude waves driven by surface phenomena (involving volumes of material similar to those of asteroids) have occurred in recent memory. Examples include the Ritter Island volcanic collapse (Ward & Day 2003) and the Lituya Bay landslide (Miller 1960a,b; Mader & Gittings 2002).

In this paper, we describe some calculations we have done of the on-shore propagation of waves that might be generated from the impact of a typical small object (of diameter $d = 300$ m). We are particularly interested in the run-up R, or the maximum on-shore elevation of wave up-rush above the still-water level (Morang & Garcia 2002). We have performed a series of calculations for a relatively simple model bathymetry $h(x)$ in one spatial dimension, a depth profile typical of the Pacific coast of North America (Le Méhauté & Wang 1996). Given the large parameter space of potential impactors and impact locations, the wide diversity of shoreline bathymetry around the world, and the potential for strong refraction due to local depth variations, we do not attempt an exhaustive characterization. We focus instead on a particular case that is representative. More elaborate calculations (for instance, involving 2-D site-specific bathymetry) may be warranted at a later date as a follow-up to the work presented here.

The sudden release of energy in a small volume in an impact strongly resembles that of an explosion. Recognition of the similarity between the two phenomena was a significant advance in understanding of impacts (Melosh 1989). Important aspects of impact tsunami may, therefore, be understood in light of the behaviour of underwater explosions (Van Dorn *et al.* 1968; Le Méhauté 1971; Le Méhauté & Wang 1996). We may divide the overall process of a deep-ocean impact tsunami into five phases: (1) initial impact of the bolide into the ocean and formation of a transient cavity in the water; (2) collapse of the cavity and propagation of large waves from the impact centre outward over deep water; (3) initial effects on wave amplitude as shallower water of the continental slope is reached (wave shoaling); (4) breaking of waves in relatively shallow water (<100 m depth) on continental shelves and (5) final contact of

waves with the shore and their progression onto dry land. An important similarity between impact tsunami and explosions, and one that makes them differ strongly from more familiar earthquake and landslide-generated tsunami, is the fact that the former are essentially surface-driven phenomena. This means that there is a wide distribution in the frequency spectrum of waves generated, compared to waves generated by seafloor bottom motion. Phases (1) and (2) of impact-driven tsunami are likely to generate waves that break near the impact point, simply due to their large amplitude. Such waves will interact with the ocean bottom, even for small impactors ($d \sim 250$ m) into deep water ($\sim$4–5 km depth).

Previous work of ours (Korycansky & Lynett 2005) has centred on phases (3) and (4), in particular the so-called 'Van Dorn effect' (Van Dorn *et al.* 1968), in which large waves due to impacts or explosions are thought to break at relatively large distances offshore and thus undergo enhanced dissipation. Korycansky & Lynett (2005) found that far-offshore breaking (at distances of several kilometres) did occur for waves of the relevant heights (tens of metres) and periods (tens of seconds up to $\sim$100 s) incident on representative coastal profiles. Breaking distances found by numerical calculations were consistent with ones predicted by a semi-analytic theory of nonlinear wave shoaling (Cokelet 1977; Sakai & Battjes 1980). It has been suggested that the Van Dorn effect operating on impact tsunami will cause sufficient dissipation of wave energy to greatly reduce onshore effects compared to previous estimates (Melosh 2003).

Modelling of impact tsunami is described by Weiss *et al.* (2006). Their strategy is broadly similar to ours: separation of the process into an impact phase (modelled by a numerical impact physics code) and a wave propagation phase (modelled by a non-linear wave code). Weiss *et al.* (2006) model the near-shore region run-up specifically using a shallow-water method based on the algorithm of Titov & Synolakis (1995).

Wave-tank experiments measuring run-up have been carried out in a number of studies (Bowen *et al.* 1968; Roos & Battjes 1976; Van Dorn 1976, 1978; Gourlay 1992; Baldock & Holmes 1999; Dijabnia 2002). We have used the results of these studies to validate the calculations in this paper, as described below. Run-up of waves on natural beaches is also relevant to our problem, particularly waves from storms that may be some metres in size. Storm wave periods can range up to $\sim$20 s, smaller than the leading waves from an impact tsunami, but still of interest for this problem. Unlike monochromatic or slowly varying wave trains, storm and other sea waves contain a broad range of frequencies, with a corresponding broad range of shoreline response. Useful measures of run-up and other wave activity are, therefore, statistical in character. For example, one characterization of run-up is R_2, the level of run-up which is exceeded by the highest 2 per cent of the waves (Holman 1986). Other measures of run-up are also in use (Morang & Garcia 2002). The spectrum of shore response is often divided into a time-independent setup level and a time-varying 'swash' about the mean. In turn the swash spectrum can be divided into a slowly varying infragravity component (frequencies $f < 0.05$ Hz) and an incident component ($f > 0.05$ Hz).

A commonly used parameter for observations and empirical analysis of run-up and other wave characteristics is the 'Irribaren number' (Hunt 1959; Battjes 1974)

$$\xi = s(H_0/L_0)^{-1/2}, \tag{1}$$

where H_0 and L_0 are the deep-water peak-to-peak waveheight and wavelength, and s is the beach slope. It was suggested that wave quantities such as run-up scale with ξ and that in particular, the ratio R/H_0 (the relative run-up) is directly proportional to ξ with a constant equal to unity:

$$\frac{R}{H_0} = \xi. \tag{2}$$

[See also Morang & Garcia (2002) and Elfrink & Baldock (2002) for further discussion of the Irribaren parameter.]

In addition to the comparisons between our calculations and laboratory experiments, it is also worthwhile to compare with observations of run-up onto beaches. There are a number of observational studies that have been made with the aim of generating predictive run-up formulae and determining the correlation (if any) with waveheight, beach slope and ξ. Examples include work by Guza & Thornton (1981, 1982), Holman (1986), Holman & Bowen (1984), Holman & Guza (1984), Holman & Sallenger (1985), Howd *et al.* (1991), Hanslow & Nielsen (1993), Raubenheimer *et al.* (1995), Raubenheimer & Guza (1996), Ruessink *et al.* (1998), Raubenheimer *et al.* (2001) and Ruggiero *et al.* (2001, 2004). A recent extensive set of observations combined with an analysis of empirical parametrizations is presented by Stockdon *et al.* (2006). We are particularly interested in situations for which ξ is small ($\xi < 0.3$), or so-called 'dissipative' beaches (Wright & Short 1984). Results seem to be mixed, in terms of which combination of parameters correlates best with the observed wave characteristics. Some studies find that R/H_0 is independent of incoming wave properties, some find the best correlation with H_0 and L_0 only independent of beach slope, and some find a significant correlation with ξ. For example, Guza & Thornton (1982) find R linear proportional to H_0 in their data, while Holman & Sallenger (1985), Holman (1986) and Howd *et al.* (1991) report run-up scaling with ξ. Other possible scalings are given by Nielsen & Hanslow (1991), who fitted R as a function of $(sH_0L_0)^{1/2}$ (in our notation) and Stockdon *et al.* (2006) who find $R \propto (H_0L_0)^{1/2}$ for small values of ξ. Ruessink *et al.* (1998) and Ruggiero *et al.* (2004) also concentrated on the regime $\xi < 0.3$ regime, and find a dependence of run-up on ξ. The most extensive recent observations are reported by Stockdon *et al.* (2006), the bulk of which covered the regime $0.3 < \xi < 4.0$, although several of their data sets had $\xi < 0.3$. Slopes fell in the range $0.005 < s < 0.025$. The 2 per cent run-up R_2 ranged up to $\sim$3.2 m over the entire data set of observed waves. Stockdon *et al.* (2006) decomposed the run-up into time-averaged wave setup and a time-variable swash component, itself divided into low-frequency infragravity ($f < 0.05$ Hz) and incident bands ($f > 0.05$ Hz). They found that setup and incident-band swash were best parametrized by a nearly linear dependence on ξ, but that infragravity swash (which dominates for $\xi < 0.3$) correlated best with offshore waveheight and wavelength only, with no dependence on beach slope. In general, the reported results for ocean waves on natural beaches differ from ours, for which we suggest that $R/H_0 \sim$ constant at low values of ξ, as seen in our results described in the following sections.

This paper extends our previous calculations to phase (5) of the impact process as defined above. In the next section we describe our method and the parameters of our calculations. We present our results in the following section, followed by our conclusions.

2 METHODS

We performed our run-up calculations using the COULWAVE code. COULWAVE solves the depth-integrated form of the Boussinesq approximation to the full Navier–Stokes equations (Nwogu 1993; Liu 1994; Wei *et al.* 1995; Kirby 1997). COULWAVE is a single-fluid code; additional interactions are not included such as those with the atmosphere (e.g. wave drag) or possible fluid portions of the

ocean bottom (e.g. bottom sediments), which may be important in run-up zones. A detailed description of the code and its validation for a number of test problems is given by Lynett *et al.* (2002). More details about the code, in particular, modifications that were made for the updated version, can be found in papers by Korycansky & Lynett (2005) and Lynett (2006, 2007), as well as Appendix A to this paper. (The version of the code used in this study is the one referred to as the 'one-layer' model by Lynett.) In particular, advective terms in the equations are sometimes partially upwinded (to a specifiable degree governed by an upwinding coefficient $0 < c_u < 1$), and a numerical viscosity term is introduced into the equations. When present, the upwind differencing has no effect on the waveform before breaking, though it adds to the stability of the model in the surf zone and improves its behaviour during simulation the run-down phase of waves at the shore. Non-zero upwinding $c_u > 0$ does have some damping effect on the run-up, so where possible we have not used it (i.e. we set $c_u = 0$). The only calculations for which upwind proved necessary were for large waves from near-shore impacts (impact distance $D = 100$ km offshore). The magnitude of the numerical viscosity is given by $\nu = \nu_0(gh_0^3)^{1/2}$, where ν_0 is a small coefficient (typically 10^{-5} in our calculations), $g = 9.81$ m s^{-2} is the gravitational acceleration, and h_0 is the depth of the water where the waves are generated. Bottom friction is modelled via a term $R_f = f_{BF}u|u|/(h + \zeta)$, where u is the fluid (not wave) velocity, $h + \zeta$ the total water depth, and f_{BF} is the friction coefficient. COULWAVE includes an eddy-viscosity model for wave breaking very similar to that described by Kennedy *et al.* (2000). Wave breaking turns on when the time-derivative $\dot{\zeta}$ of the surface elevation is larger than a critical value $\dot{\zeta}_c = 0.65c_0$, $c_0 = [g(h + \zeta)]^{1/2}$. The breaking is turned off when $\dot{\zeta}$ falls below $\dot{\zeta}^*$, a criterion whose time-dependent value is given in detail in Appendix A. The coefficients of the wave-breaking model were calibrated by comparison to the experiments of Hansen & Svendsen (1979). Additionally, Lynett (2006) presented validation calculations of one- and two-layer models with experimental data for wave-breaking over a submerged step (Dingemans 1994), laboratory experiments of cnoidal waves breaking on a planar slope (Ting & Kirby 1995, 1996), and metre-scale field data from the SwashX experiments (Raubenheimer 2002).

COULWAVE includes several kinds of wave-driver terms. The ones we have used are monochromatic sinusoidal waves and a driver term E_s that is proportional to the amplitude of an input surface time-series. We used the latter for the input tsunami wave trains from the linear theory described by Ward & Asphaug (2000).

3 RESULTS

We first present some results comparing the performance of COULWAVE against run-up measurements from wave-tank experiments of monochromatic waves. We then present our results of run-up calculations of wave trains generated by impact tsunami (or more precisely, wave trains generated by the collapse of cavities resulting from models of impacts into deep water). The subsections of this portion of the paper follow the sequence of different sets of calculations that we carried out.

3.1 Laboratory-scale monochromatic waves onto simple slopes: comparison with experiments

We have collected experimental results of wave run-up from monochromatic waves from the literature (Bowen *et al.* 1968; Roos & Battjes 1976; Van Dorn 1976, 1978; Gourlay 1992; Baldock & Holmes 1999; Dijabnia 2002). The experiments were measurements of the run-up R of decimetre-scale waves in wave tanks onto simple slopes of steepness s ranging from $s = 0.022$ (Van Dorn 1976, 1978) to $s = 1/3$ (Roos & Battjes 1976). For our analysis we take the given wave periods T and compute the deep-water wavelength $L_0 = gT^2/(2\pi)$. In the cited papers, waveheights are sometimes given as measured height H uncorrected for shoaling to the deep-water value H_0; in such cases we have applied the linear-theory correction for H_0, given by

$$H_0 = SH, \qquad S = (\tanh kh + kh/\cosh^2 kh)^{1/2}, \tag{3}$$

where k is the wavenumber satisfying the linear dispersion relation $L_0 = 2\pi k \tanh kh$. As will be seen below, the Irribaren scaling relationship (Battjes 1974) appears to match the experiments quite well over nearly two orders of magnitude in ξ. [However, Jordaan (1972) presents results suggesting a different power law, with run-up independent of slope for $s = 1/15$ and $1/30$: $R/H_0 = 0.34(H_0/L_0)^{-1/3}$.]

For comparison with experiments and check the performance of COULWAVE we calculated run-up on to a simple slope for a hundred combinations of slope s, wavelength L, and waveheight H in a model wave tank of depth $h = 1$ m. Parameters were chosen from the following sets: $s = [0.01, 0.02, 0.05, 0.1 \text{ and } 0.2]$, $L = [2, 5, 10 \text{ and } 20]$ m, and $H = [0.01, 0.02, 0.05, 0.1 \text{ and } 0.2]$ m. We set the bottom friction f_{BF} to zero but included a modest amount of dissipation $\nu_0 = 10^{-3}$. Resolution was typically 100–200 points per driving wavelength L. Fig. 1 shows a small sample of results from the set of the calculation: time-series of the run-up for five calculations as shown. The run-up R is plotted as a function of time, where R is defined as the height of the intersection of the water level with the beach slope above the undisturbed level. Fig. 1 shows a very typical behaviour exhibited in many of the runs: an initial peak transient run-up that was sometimes several times larger than the oscillatory quasi-steady state. The transient is particularly evident in for the shallow-slope calculations $s = 0.01$ and 0.02, although the precise manifestation also depends on the driving-wave characteristics. Large amplitude waves also show a more prominent initial peak run-up. We attribute this to non-linear response to the impulsive start of the wave train. We assume that the experimental results were measurements of the steady state. We therefore, measured the maxima of the steady portion of the responses and took that to be the relevant result for experimental comparison. Included in Fig. 1 are the corresponding values of the Irribaren parameter $\xi = s(H_0/L_0)^{-1/2}$. To anticipate the results of Fig. 2, we see that generally $R/H \approx \xi$, with the discrepant example of panel (a), in which the run-up is several times larger than predicted by the scaling law.

Fig. 2 shows the experimental measurements of the relative run-up R/H_0 versus the scaling parameter ξ compared with those from the COULWAVE calculations. The relation $R/H_0 = \xi$ is plotted in each panel to guide the eye. Panel a) shows the measurements from the cited literature; it is seen that the simple relation given in eq. (2) is a good description of the results over nearly two orders of magnitude of ξ. We should mention also the measurements made by Bruun & Günbak (1977), onto steep slopes ($s = 1/3$, 1/2 and 2/3), for the $1.3 < \xi < 8$, which overlaps the range of ξ in Fig. 1. Bruun & Günbak found that relation (2) held for $\xi < 3$, above which R/H_0 was constant or slightly declining at a value of $\sim$2. Waves that followed the scaling relation produced plunging breakers on the slope, while waves associated with larger values of ξ and smaller run-up were collapsing or surging breakers. Panels (b)–(f) show COULWAVE results for all combinations of H_0 and L_0 the respective slopes $s = 0.01 - 0.2$ as labelled. For the COULWAVE results displayed in Fig. 2, we converted H and L to the deep-water values H_0 and L_0 for the numerical wave tank depth $h = 1$ m.

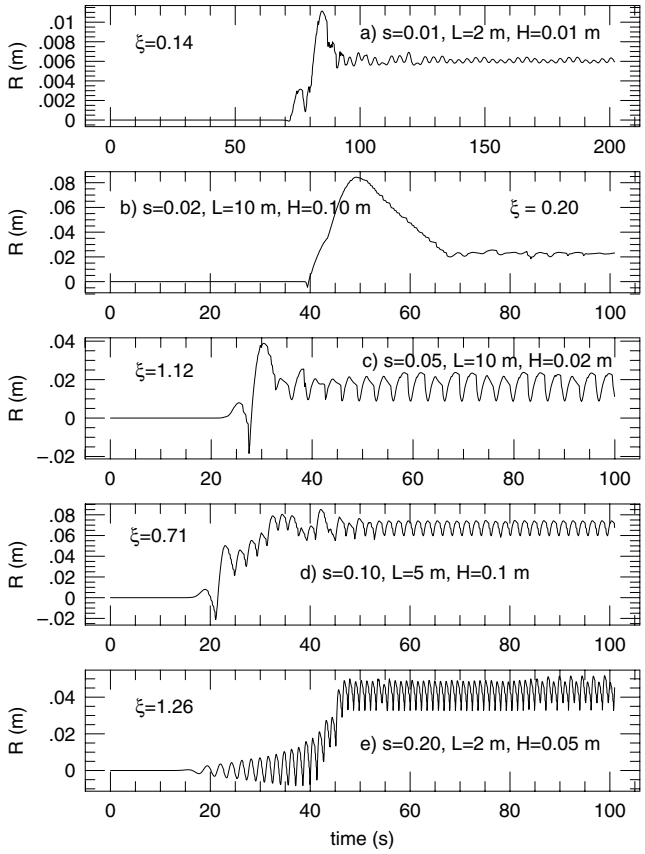

Figure 1. Sample results of our calculations of the run-up of monochromatic waves onto simple slopes. The run-up R in metres is plotted as a function of time. The undisturbed water depth is $h = 1$ m. The viscosity $\nu = 10^{-3}$ and the bottom friction was set to zero. The resolutions of the calculations was 100 gridpoints per wavelength L. The slope s of the beach, wavelength L waveheight H and corresponding values of ξ are given in each plot. Panel (a) $s = 0.01$, $L = 2$ m, $H = 0.01$ m, $\xi = 0.14$; (b) $s = 0.02$, $L = 10$ m, $H = 0.1$ m, $\xi = 0.20$; (c) $s = 0.05$, $L = 10$ m, $H = 0.02$ m, $\xi = 1.12$; (d) $s = 0.1$, $L = 5$ m, $H = 0.1$ m, $\xi = 0.71$ and (e) $s = 0.2$, $L = 2$ m, $H = 0.05$ m, $\xi = 1.26$.

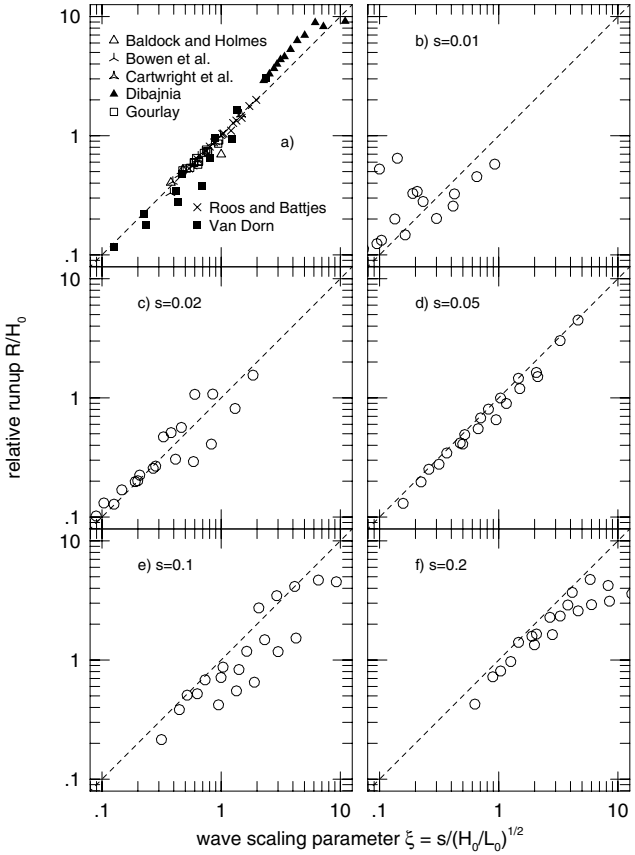

Figure 2. Wave-tank experimental measurements of run-up from the literature and COULWAVE run-up results (open circles). The relative run-up R/H_0 is plotted versus the wave scaling parameter $\xi = s(H_0/L_0)^{-1/2}$. Panel (a) Experiments (b) COULWAVE runs with $s = 0.01$ (c) COULWAVE runs with $s = 0.02$ (d) COULWAVE runs with $s = 0.05$ (e) COULWAVE runs with $s = 0.1$ (f) COULWAVE runs with $s = 0.2$.

Generally speaking, the performance of COULWAVE in this problem is quite satisfactory. A fit to the numerical results (forcing R/H_0 to be proportional to ξ) yields $R/H_0 = 0.85\xi$. We see that there is greater deviation from the eq. (2) for $s = 0.1$ and 0.2. Likewise, results for the shallowest slope $s = 0.01$ show some scatter which seems to result in systematically larger run-up than predicted by Irribaren scaling. This tendency persists and indeed becomes more prominent for the calculations presented below.

The experimental results sample relatively large slopes and values of ξ, compared to the tsunami regime of primarily interest to us. Only Van Dorn (1976, 1978) and Dijabnia (2002) report results for $s < 0.05$, and all experiments have $\xi \geq 0.4$ except for those by Van Dorn, whose data extend down to $\xi = 0.12$. The low-Irribaren regime is of primary interest to us. This regime is described by Elfrink & Baldock (2002) as 'saturated', in which we may expect low-frequency changes in the water level (also known as wave setup or infragravity wave energy) to dominate the time-behaviour of the run-up. Our results bear this out, as will be apparent below.

In the next sections, our aim is to disentangle the effects of different factors: large amplitude and variable amplitudes, wavelengths and slopes. Impact tsunami wave trains have continuously variable amplitudes and wavelengths. Bathymetry profiles will have non-constant slopes. The applicability of the Irribaren scaling formula to run-up becomes less obvious in these circumstances. We have made choices for the factors in the formula that seem to work reasonably well, as discussed below.

3.2 Large monochromatic waves onto simple slopes

The next set of calculations we present are of large-amplitude (waveheights of 10, 20, 50 and 100 m), long-period (20–80 s) waves onto shallow slopes ($s = 0.005$, 0.01 and 0.02). Irribaren numbers fall in the range $0.0559 < \xi < 0.663$. The wave properties are typical of the waves that might be generated by the impact of a subkilometre diameter object into deep water (i.e. a depth $h \sim 4-5$ km). The slopes are also typical of bathymetric profiles of interest, and are also shallower than is usually constructed in wave tanks. Shallow-slope calculations are challenging as well. A shallow slope means a long run of wave propagation, and the concomitant shortening of waves as they propagate into water of slowly decreasing depth means that high resolution is required, typically hundreds of points per deep-water wavelength L_0. Our goal for these specific

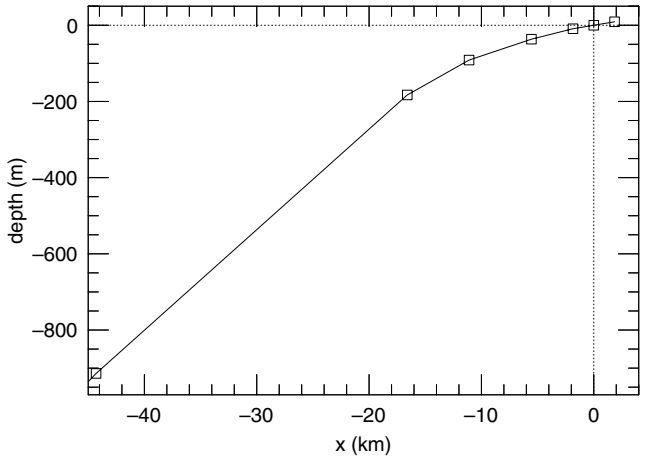

Figure 3. Pacific coast depth profile used in the tsunami run-up calculations. The profile is a piecewise-continuous interpolation of the data given by Le Méhauté & Wang (1996). The calculations discussed in the text start at 800 m depth, approximately 40 km from shore except as indicated.

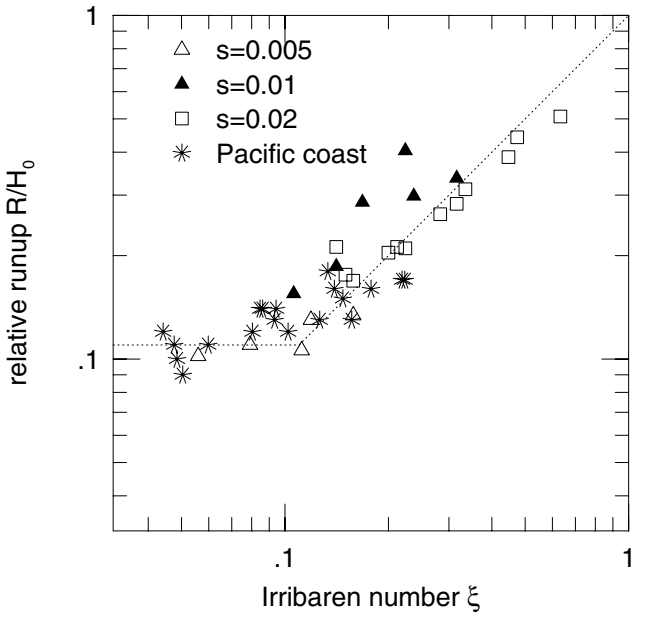

Figure 4. The relative run-up R/H_0 plotted versus Irribaren number $\xi = s(H_0/L_0)^{-1/2}$ for monochromatic waves of large amplitude (10–100 m) and long periods 20–80 s for slopes $s = 0.005$, 0.01 and 0.02) as indicated, along with results for waves propagating on to the Pacific Coast bathymetry profile shown in Fig. 3. The dotted line is a piecewise-linear fit to the results: $R/H_0 = \xi_0(\xi < \xi_0)$, $R/H_0 = \xi$ $(\xi \geq xi_0)$, for $\xi = 0.11$.

calculations was to see if run-up is scale-independent. The basic fluid dynamic equations are independent of scale, being governed by dimensionless parameters such as Reynolds and Froude numbers. Code parameters such as those involved in the wave-breaking model in COULWAVE might introduce scale effects, however. The wave-breaking model was calibrated using the results of centimetre-scale laboratory experiments, and might conceivably show different behaviour for waves of heights of tens of metres. Results from these calculations are plotted in Fig. 4, along with the results from the next set of calculations.

3.3 Large monochromatic waves onto Pacific coast profile

In this section, we discuss calculations of wave propagation onto a compound-slope bathymetry profile that is representative of the Pacific coast of North America. Fig. 3 shows the bathymetry profile, from Le Méhauté & Wang (1996). For waves propagating onto a compound slope, we must choose a value of s, if characterizing the results in terms of ξ. We have chosen to take the average value of the slope from the point where the waves break: $s = s_b = h_b/x_b$, where h_b is the water depth and x_b is the distance from shore of the breaking point. We note that this choice is *a priori* (just as with similar choices for H_0 and L_0 in subsequent calculations), rather than *post hoc* fits that maximize the correspondence between ξ and R/H_0. For these calculations, the slopes range from $s_b = 0.00558 - 0.0115$ and ξ covers the range $0.044 < \xi < 0.22$.

These particular calculations were carried out for the study by Korycansky & Lynett (2005) of off-shore breaking by large waves (the Van Dorn effect). Wave run-ups were monitored, but were not reported in that paper. Fig. 4 shows the relative run-up R/H_0 versus, for both the calculations of the preceding section (large monochromatic waves onto simple slopes) and the same waves onto the Pacific coast profile. Overall, the agreement with the predictions of Irribaren scaling is satisfactory. There is a fairly clear tendency for R/H_0 to depart from Irribaren scaling for $\xi \leq 0.1$, in the sense that the run-up is larger than predicted by the scaling. This trend persists for the other calculations that we discuss below.

A piecewise-linear fit to the results in Fig. 4 is:

$$\frac{R}{H_0} = \begin{cases} \xi_0, & \xi < \xi_0, \\ \xi, & \xi \geq \xi_0. \end{cases} \tag{4}$$

A least-square analysis gives $\xi_0 = 0.11$.

3.4 Scaled impact tsunami wave trains onto simple slopes

We next turn to calculations of the run-up from impact tsunami. As noted above, our aim in this paper is to determine the run-up from a typical situation or a generic impact. The parameters of the impact (chiefly impactor size and the location of the impact) vary over large ranges and produce highly location-specific results. A detailed study of a specific scenario would be a fairly massive effort. Even the 1-D calculations that we present here, involving a generic ocean depth profile, are challenging We thus focus on a representative case, namely a 300-m diameter object striking into deep water ($h = 4$ km) off the Pacific coast of North America.

The source terms in the calculations are wave trains (surface traces) from linear-theory models of the ocean response to an asteroid impact, as in calculations by Ward & Asphaug (2000). The wave trains are generated by the collapse of a parabolic cavity in deep water, whose shape (depth and radius) are obtained from a scaling relation. The far-field wave trains are characterized by dispersive wave packets that last for many minutes at distant locations. Individual waves in the first group have periods of ranging from ∼60 to 120 s, with wave periods decreasing as the group passes by a fixed point, as expected from the dispersion relation for water waves. The first group or packet has the highest amplitude, so we have limited the duration of calculation to cover only the arrival of the first packet, as we are interested in the maximum run-up produced by the waves. Input wave trains from a sample of the offshore impact locations are shown in Fig. 5, which shows the surface $\eta(t)$ as a function of

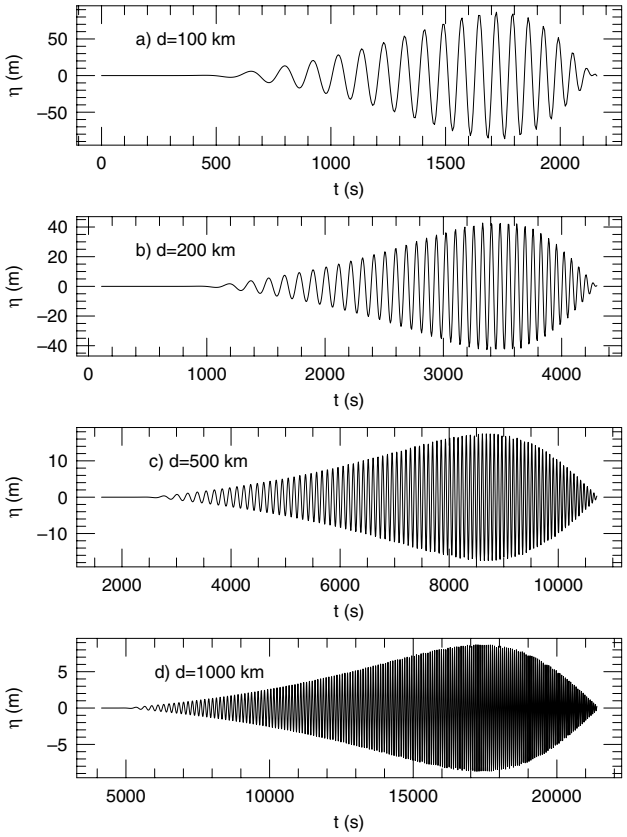

Figure 5. Ocean surface inputs for run-up calculations: The surface η as a function of time at the indicated distances from the impact point of a 300-m diameter object striking the ocean surface at 20 km s^{-1}. Only the first group of the wave train was used in the calculations, as shown.

time at specified fixed distances from the impact point for a 300-m diameter object. The maximum peak-to-trough waveheight $H_{\max}$ is inversely proportional to the distance due to a combination of geometrical spreading and dispersion, as predicted by linear theory. In this particular case we have $H_{\max} \approx 174(100\,\mathrm{km}/D)$ m.

Numerical hydrodynamic simulations by Gisler *et al.* (2003) present a different picture of wave generation from impacts. They simulated impacts by objects of sizes from 250 m to 1 km. They also performed 3-D calculations of 1-km diameter iron asteroids at a velocity of 20 km s^{-1} into a 5-km deep ocean, at angles of 45° and 60° from the vertical. The wave trains are complex and nonlinear, showing overturning waves. The simulations do not show the long modulated wave trains expected from linear-theory calculations of the collapse of a cavity. Gisler *et al.* (2003) also find that the waves decay faster than the linear-theory prediction of r^{-1} from the impact point.

At the present writing it is not clear which type of wave train is a more accurate picture of the impact tsunami waves. The answer may depend on the size of the impact. One may expect long dispersive wave trains from smaller impacts. Modulated wave trains have been found in explosion tests (Van Dorn 1961; Van Dorn *et al.* 1968; Le Méhauté 1971; Le Méhauté & Wang 1996) as well as the relatively slow ($\propto r^{-5/6}$) decay of waves from megaton-yield nuclear tests (Van Dorn 1961). We have chosen to work with dispersive linear waves as the more conservative case, given their slow decay with distance and long-time persistence. We focus on relatively small impactors as we may expect them to generate the largest frequency of multimetre run-ups (Ward & Asphaug 2000). Nonetheless, it should be recognized that, as noted above, our initial conditions represent an idealized case, and that large waves from an impact are likely to break near the impact centre, as found by Gisler *et al.* (2003), leading to a more complicated wave train.

In the calculations we used the surface amplitude time-series $\eta(t)$ as a source in the equation for the water depth $\zeta(x, t)$. We found that using a simple driver term E_s that was proportional to η produced satisfactory results:

$$E_s(x, t) = \left(\frac{2\pi\Delta t}{P}\right) C\eta(t) e^{-\beta(x-x_0)^2}, \tag{5}$$

where P is the period of a wave of wavelength L in water of depth h, C is an empirically determined coefficient of order unity, and β determines the width of the source around the location x_0. The spatial form of E_s is the same as that in the more elaborate source model of Chawla & Kirby (2000). For our calculations, we chose characteristic values $L = 10^4$ m and $h = 10^3$ m, which are order-of-magnitude values of the longest waves and water depths in our simulations. The value of L comes from impact scaling of water cavity diameter for the impact of a 300-m bolide and h is the order of magnitude of the depth at the input boundary of the grid. The resulting value of $P = 107$ s is typical of the individual waves in the packets shown in Fig. 5. The source location x_0 was set at the 800-m depth level in the profile shown in Fig. 3, corresponding to a distance $x_0 = -40$ km from the undisturbed shoreline at $x = 0$. We set $\beta = 100/L^2$ and found that a value of $C = 0.85$ worked well, as determined by matching the surface response $\zeta(x_0, t)$ at $x = x_0$ with the original time-series $\eta(t)$.

Running COULWAVE with the surface driver E_s generates a series of waves that propagates toward the shore. (Waves also propagate in the opposite direction $x < x_0$, but an absorbing 'sponge layer' boundary condition with a thickness of $1.25L$ at the end of the grid damps the waves and prevents wave reflection.)

A snapshot of propagating waves from one particular calculation is shown in Fig. 6. The wave source corresponds to an impact at distance of 400 km from the 800-m location. The surface $\zeta(x, t)$ is shown at $t = 8100$ s, at a time when the run-up is near its maximum. Dotted lines in the plot show the bathymetry $h(x)$. The resolution of the grid is $\Delta x = 12.5$ m, or 800 points per nominal wavelength L. High resolution is required due to the shortening of waves as the water depth becomes small at the shore, as can be seen in Fig. 6. In this particular calculation the numerical viscosity coefficient $\nu_0 = 10^{-5}$ ($\nu \approx 1$ m s^{-2}), and the bottom friction f_{BF} was set to zero. The same wave series is shown in all three panels of Fig. 6 in order to emphasize the character of ζ at different scales. In panel (a), we see the overall wave train, increasing in amplitude until it breaks at $x \approx -12$ km at this particular moment. The breaking zone extends inward to about 200 m from shore. Panel (b) shows the wave train deep inside the breaking zone. Broken waves have become propagating bores with steep leading edges that eventually break into undulating bores. In panel (b) we also see an strong wave set-up level of ~5 m that comprises the greater part of the run-up. Panel (c) shows the inner 1.5 km of the waves, after the bores have broken into an undulating form and reformed into a non-broken wave train. The symbols on the wave train mark the location of gridpoints and show that the short waves at the shore are moderately well resolved in the calculation. For this case, $\xi = 0.134$ based on the H_0 and L_0 of the maximum part of the wave train and the average slope shoreward of the breaking point.

Resolution and convergence are always important concerns in calculations of this kind. We have addressed this issue by running simulations at different grid resolutions. Grid resolutions in the

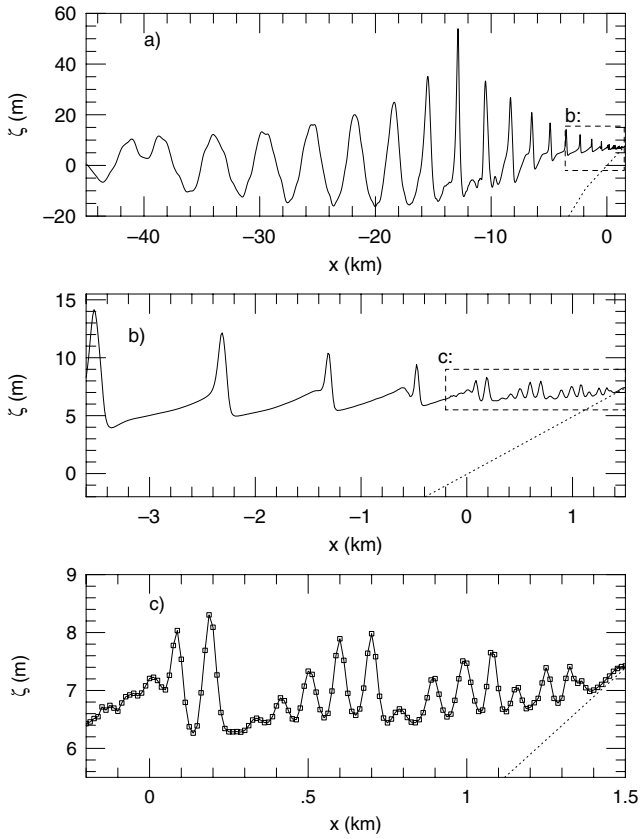

Figure 6. Waveheight ζ as a function of distance x for $t = 8100$ s for the case in which the impact is 400 km distant from the 800-m depth mark on the grid. The same wave train is shown in all three panels, but is plotted at different scales in each one. The location of the undisturbed shoreline is $x = 0$. The dotted line is the bathymetry profile. The dashed box in panel (a) is an inset of panel (b) as indicated. Likewise, the dashed box in panel (b) is an inset of panel (c). In panel (c), the open symbols show the location of gridpoints. For this case, $\xi = 0.134$ based on the H_0 and L_0 of the maximum part of the wave train and the average slope shoreward of the breaking point.

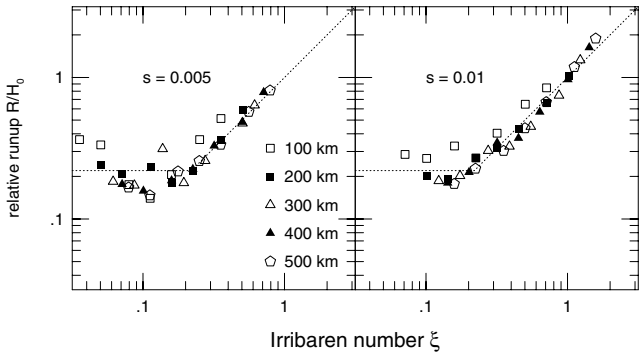

Figure 7. Relative run-up R/H_0 plotted versus Irribaren number $\xi = s(H_0/L_0)^{-1/2}$ for scaled tsunami wave trains onto simple slopes $s = 0.005$ and 0.01. The dashed line is the piecewise linear fit $R/H_0 = \xi_0(\xi < \xi_0)$, $R/H_0 = \xi$ $(\xi \geq \xi_0)$, for $\xi = 0.22$.

calculations ranged from 100 m down to 6.67 m in the x-direction. (Vertical resolution is of course undefined for one-layer calculations.) We tested various resolutions for the calculation of tsunami wave trains on the Pacific coast profiles described below. Run-up

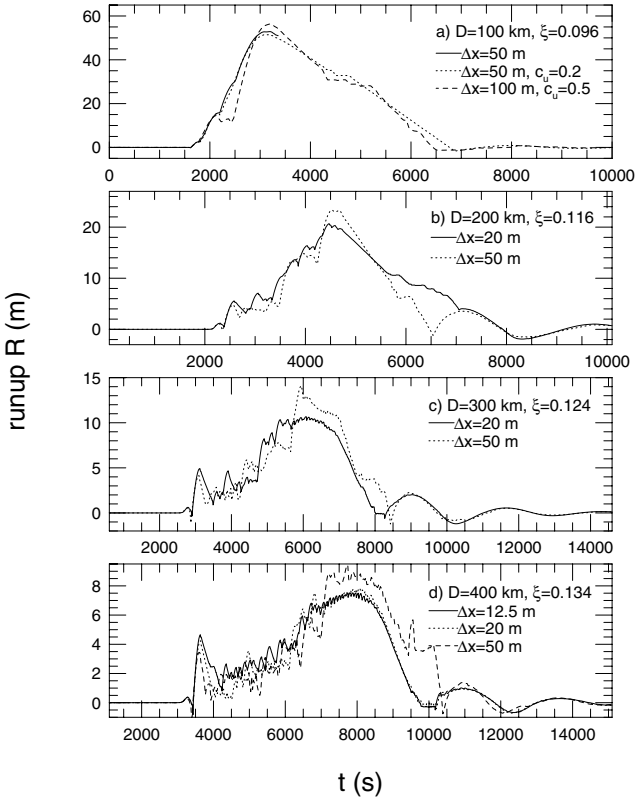

Figure 8. Run-up R as a function of time for the wave trains generated by the impact of a 300-m diameter object into deep water, for various distances from the impact site. The distance D is the distance from the impact site to the 800-m depth mark. Calculations are shown for various grid resolutions Δx. All calculations were made with numerical viscosity coefficient $\nu_0 = 10^{-5}$ (or numerical viscosity $\nu = 1$ m s^{-1}) and bottom friction coefficient $f_{bf} = 0$. Except where noted, the upwinding coefficient $c_u = 0$. (a) $D = 100$ km. Solid line: $\Delta x = 50$ m, dotted line: $\Delta x = 50$ m, $c_u = 0.2$, dashed line: $\Delta x = 100$ m, $c_u = 0.5$. (b) $D = 200$ km. Solid line: $\Delta x = 20$ m, dotted line: $\Delta x = 50$ m. (c) $D = 300$ km. Solid line: $\Delta x = 20$ m, dotted line: $\Delta x = 50$ m. (d) $D = 400$ km. Solid line: $\Delta x = 12.5$ m, dotted line: $\Delta x = 20$ m, dashed line: $\Delta x = 50$ m. Values of ξ are as indicated based on the H_0 and L_0 of the maximum part of the wave train and the average slope shoreward of the breaking point.

traces as functions of time at different resolutions are shown in Figs 8 and 9 to illustrate the degree of convergence and to indicate the reproducibility and uncertainty in the results. The different resolutions used for calculations at each distance D are indicated in the captions to Figs 8 and 9. Generally speaking, resolution of 20 m or finer gives reasonably reliable results. We have found, however, that the resolution cannot be increased beyond a certain value in a given calculation. Breaking waves become too steep on the grid and the calculation breaks down. The breakdown resolution depends on the amplitude of the waves involved; larger waves cause the breakdown to occur sooner. However, convergence is usually reached before the breakdown point. This points to the limitations of our model governing equations: at high resolutions, the shortest waves on the grid ($L = 2\Delta x$) have large values of kh for which the solution scheme behaves poorly. So long as the solution remains smooth, this problem is not an issue. The growth of $2\Delta x$ waves can be controlled to some extent by the use of upwinding as mentioned above. However, too large a value of upwind coefficient c_w damps the run-up.

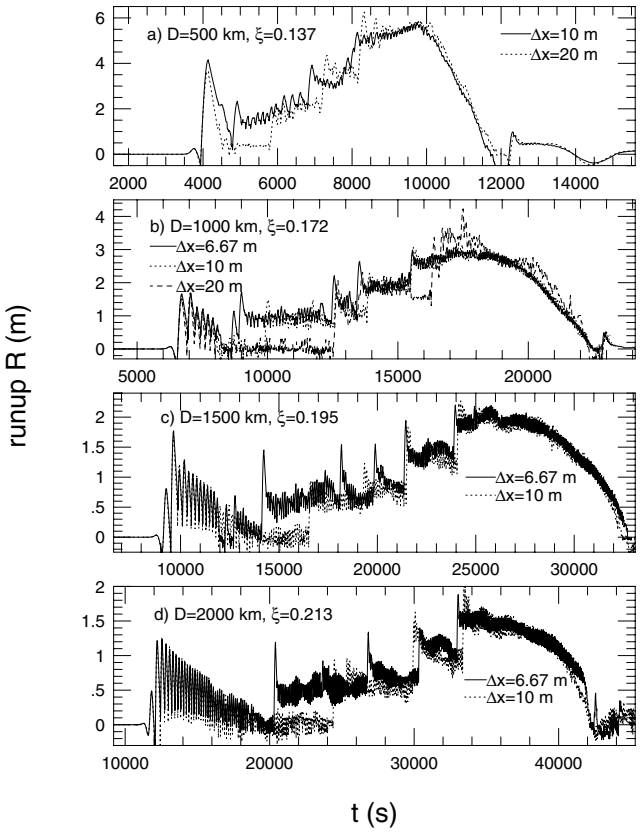

Figure 9. Run-up R as a function of time for the wave trains generated by the impact of a 300-m diameter object into deep water, for various distances from the impact site. The distance D is the distance from the impact site to the 800-m depth mark. Calculations are shown for various grid resolutions Δx. All calculations were made with numerical viscosity coefficient $\nu_0 = 10^{-5}$ (or numerical viscosity $\nu = 1$ m s^{-1}) and bottom friction coefficient $f_{bf} = 0$, and upwinding coefficient $c_u = 0$. (a) $D = 500$ km. Solid line: $\Delta x = 10$ m, dotted line: $\Delta x = 20$ m. (b) $D = 1000$ km. Solid line: $\Delta x = 6.67$ m, dotted line: $\Delta x = 10$ m. dashed line: $\Delta x = 20$ m. (c) $D = 1500$ km. Solid line: $\Delta x = 6.67$ m, dotted line: $\Delta x = 10$ m. (c) $D = 2000$ km. Solid line: $\Delta x = 6.67$ m, dotted line: $\Delta x = 10$ m. Values of ξ are as indicated based on the H_0 and L_0 of the maximum part of the wave train and the average slope shoreward of the breaking point.

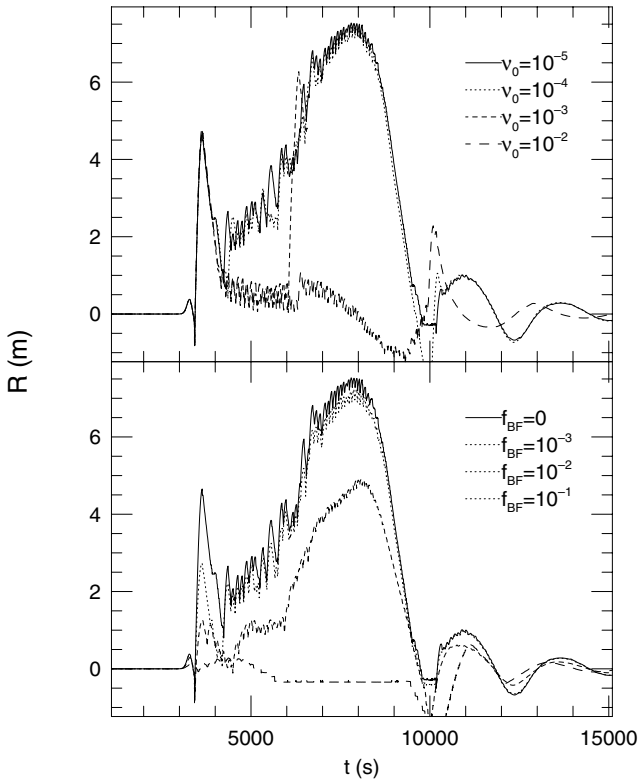

Figure 10. Run-up R as a function of time for the $D = 400$ km impact, for different values of viscosity coefficient ν_0 and bottom friction f_{BF}. Top panel: Run-up for $10^{-5} < \nu_0 < 10^{-2}$. Solid line: $\nu_0 = 10^{-5}$. Dotted line: $\nu_0 = 10^{-4}$. Dashed line: $\nu_0 = 10^{-3}$. Long dashed line: $\nu_0 = 10^{-2}$. Top panel: Run-up for $0 < f_{BF} < 10^{-1}$. Solid line: $f_{BF} = 0$. Dotted line: $f_{BF} = 10^{-3}$. Dashed line: $f_{BF} = 10^{-2}$. Long dashed line: $f_{BF} = 10^{-1}$.

For impact wave trains onto simple slopes, s is constant while H_0 and L_0 vary with time (or position along the wave train), due to the multifrequency character of the source and dispersion of the waves as they propagate. In order to compare run-up with the Irribaren number, it is necessary to choose characteristic values of H_0 and L_0 for evaluation of ξ. As noted by Ward & Asphaug (2000), the wavelength L_0 at peak tsunami amplitude correspond quite closely with the diameter of the impact cavity. Our impactor diameter (300 m) generates a cavity of 8×10^3 m in diameter according to the crater scaling rule used by Ward & Asphaug (2000). For the run-up scaling, inspection of the wave trains yields $L_0 = 8.8 \times 10^3$ m with a corresponding period of 75 s. Energy-conserving waves propagate in deep water with unchanging period, so we used the same wave of L_0 for all our run-up scaling comparisons. As for the waveheight H_0, we used the maximum value in the (scaled) wave train $bH_{\max}$, where $0 < b < 1$ is a scaling factor.

We carried out calculations using wave trains for impact distances $D = 100$, 200, 300, 400 and 500 km onto slopes $s = 0.005$ and 0.01. The wave trains were artificially scaled by factors $0.01 < b < 1$ to reduce the amplitude of the wave trains, in order to span a wider range of conditions (and Irribaren number ξ). In particular, we have used b-values of 0.01, 0.02, 0.05, 0.1, 0.2, 0.5 and 1.0 to generate a set of 35 calculations for each slope s. Irribaren numbers fall in the range $0.0356 < \xi < 1.58$. The numerical viscosity coefficient was set to $\nu_0 = 10^{-5}$ ($\nu \approx 1$ m s^{-2}), and the bottom friction f_{BF} was set to zero. The wave profiles and run-up traces looked similar to those produced full-amplitude/bathymetric runs described in the next section. Therefore, we present detailed results for latter cases only, in Figs 7–10.

We chose a depth of 800 m as the starting point of the calculations as a compromise between minimizing the amount of calculation and the neglect of possible shoaling and dispersion effects from deep water to the 800-m level. Linear wave theory shows that the amplitude change (increase or decrease) of waves of periods 60–120 s from deep water to 800 m is ≈10 per cent or less. Potentially of more effect is the change in wavelength; sinusoidal waves shorten by factors of up to 2 when travelling from deep water to 800 m depth. This may affect the dispersion of the wave packets as they propagate from the impact, so that the form of the packets will be somewhat different from the source we used.

Additionally, we have neglected radial (geometrical) spreading over the 40 km range of our calculation from 800 m to the shore. This is probably unimportant except perhaps for the very closest impacts ($D = 100$ or 200 km). For the $D = 100$ km impact we might expect a geometrical spreading factor of $(140/100)^{-1/2} = 0.85$, and a similar factor of 0.91 for $D = 200$ km.

The results (R/H_0 versus ξ) for scaled wave trains are shown in Fig. 7. The resolution of the calculations was same as that of the

highest-resolution cases for full-amplitude wave trains on the Pacific coast profile (the calculations in the next section). As with the full-amplitude calculations, the number viscosity was set to $\nu_0 = 10^{-5}$ and the bottom-friction coefficient was $f_{BF} = 0$. The results shown in Fig. 6 suggest that Irribaren scaling ($R/H_0 = \xi$) breaks down for small values of ξ. The effect seems to be stronger for $s = 0.005$ than $s = 0.01$. Fitting the piecewise formula eq. (3) yields $\xi_0 = 0.22$.

3.5 Impact tsunami wave trains onto Pacific coast profile

Finally, we look at the results for full-amplitude wave trains onto the Pacific coast profile. For these calculations, all three Irribaren scaling coefficients s, H_0 and L_0 were chosen as in the relevant calculations above ($s = h_b/x_b$, H_0 and L_0 from the linear wave train sources).

We carried out calculations for impact distances $D = 100$, 200, 300, 400, 500, 1000, 1500 and 2000 km, with Irribaren parameters $0.096 < \xi < 0.213$. We also tested the effects of different values of viscosity coefficient ν_0 and bottom friction f_{BF}. The numerical viscosity should be set to a value small enough so as not to influence the results. We found that $\nu_0 = 10^{-5}$ was satisfactory. Bottom friction is a physical parameter and typically is thought to have a non-zero value $10^{-3} < f_{BF} < 10^{-1}$ depending on the character of the ocean bottom. We have carried out calculations with f_{BF} in that range and also $f_{BF} = 0$ to find an upper limit to the run-up. Aside the those parameters, the only parameters that influence the results are those involved in the breaking model, by which the rate at which breaking waves lose energy is controlled. As noted above, the breaking-model parameters have been calibrated by experimental results in wave tanks. Finally, we made calculations at differing resolutions to assure that the run-up results would be at least moderately well converged. This was generally possible, except perhaps for the largest waves and run-ups generated by the 100-km distant impacts.

Fig. 8 shows the run-up R as a function of time for the four closest locations $D = 100$, 200, 300 and 400 km, while Fig. 9 gives the same results for $D = 500$, 1000, 1500 and 2000 km. The horizontal scale is the time after the impact in seconds and includes the time taken by the first wave group to propagate from the impact point ($D = 0$). As we have calculated the response to the first wave group only (as shown in Fig. 5), the run-up goes to zero after those waves pass through the grid. All calculations shown in Figs 8 and 9 were carried out with $\nu_0 = 10^{-5}$ and $f_{BF} = 0$. A notable feature of the results shown in Figs 8 and 9 is the gradually increasing degree of short-wavelength, high-frequency oscillations in the run-up traces as the driving wave amplitude decreases and ξ increases. This is very apparent in run-up traces (not shown here) for the scaled wave trains of the previous section. This result is compatible with known swash-zone dynamics (Elfrink & Baldock 2002; Ruggiero *et al.* 2004). Transient 'spikes' in the run-up also occur, most notably in the $D = 1500$ and 2000 km calculations. These may be due to the highly non-linear run-up process, although numerical effects cannot be ruled out.

Ideally, bottom friction values would be set from full hydrodynamic models run under various conditions, including the effects of unconsolidated sediment and the associated drag produced by turbidity currents, which may dominate other effects of seafloor roughness, particular in shallow regions. Such effects are likely to be highly variable geographically. An additional effect that we do not include in this work is the drag induced by interactions with the atmosphere, as are present in full simulations like those carried out by Gisler *et al.* (2003).

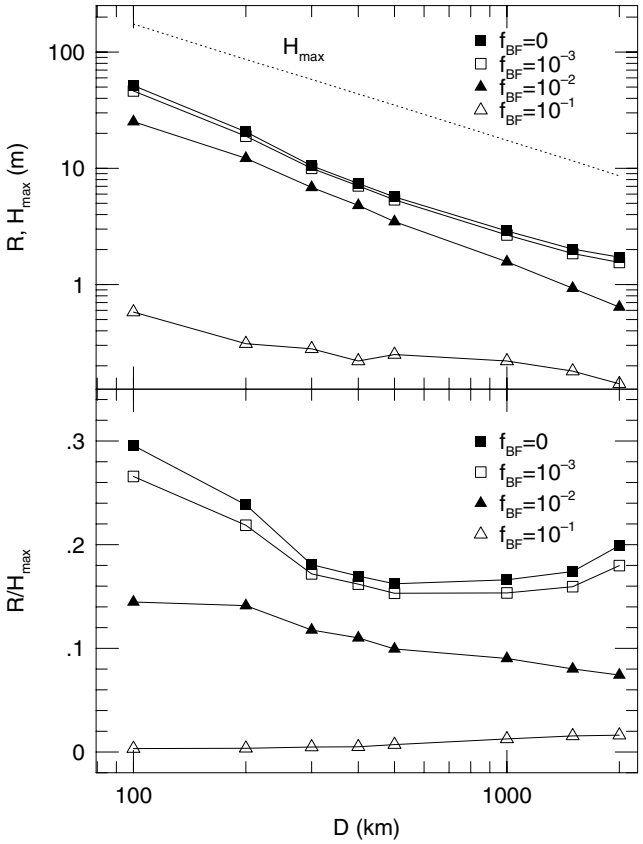

Figure 11. Run-up R (and maximum waveheight $H_{\max}$) as a function of distance D from the impact site to the 800-m depth mark. Top panel: R versus D for values of bottom friction $f_{BF} = 0$, 10^{-3}, 10^{-2}, and 10^{-1}. Also shown is $H_{\max}$. Bottom panel: the ratio $R/H_{\max}$ versus D for the same values of bottom friction.

In Fig. 10, we look at the effects on run-up of the numerical viscosity coefficient ν_0 and bottom friction f_{BF}. Both panels show the run-up R as a function of time for the $D = 400$ km distant impact. In the top panel, we see that R is not sensitive to numerical viscosity for $\nu_0 < 10^{-4}$ ($\nu < 10$ m s^{-1}.) In the bottom panel, bottom friction less than 10^{-3} does not strongly affect R. A bottom friction value of 10^{-2} does make a significant difference, and a relatively rough ocean floor $f_{BF} = 10^{-1}$ virtually eliminates the run-up altogether.

From Figs 8 and 9, we measured the maximum run-ups R, which are plotted against D in Fig. 11. Run-ups are plotted for values of bottom friction $f_{BF} = 0$, 10^{-3}, 10^{-2} and 10^{-1}. Also plotted are the maximum waveheights $H_{\max}$ of the waves that drive the run-ups. As a function of distance, $H_{\max} \propto D^{-1}$, and we see that R is also roughly proportional to D^{-1}. The lower panel plots the ratio $R/H_{\max}$ versus D; for $D > 300$ km, $R \sim 0.17 H_{\max}$ for low values of bottom friction. For a moderate value $f_{BF} = 10^{-2}$, R drops by about 40 per cent, and is essentially nil for $f_{BF} = 10^{-1}$.

In line with the previous discussion, we plot R/H_0 versus ξ for the full-scale tsunami wave trains in Fig. 12. Overall, the results are consistent with those for the scaled wave trains propagating onto simple slopes. The sequence of results does show a systematic trend in deviation from the line $R/H_0 = \xi$ but the values do not fall outside the envelope of the scaled-wave train results. The trend could result from an incorrect choice of coefficient s, which was chosen *a priori*

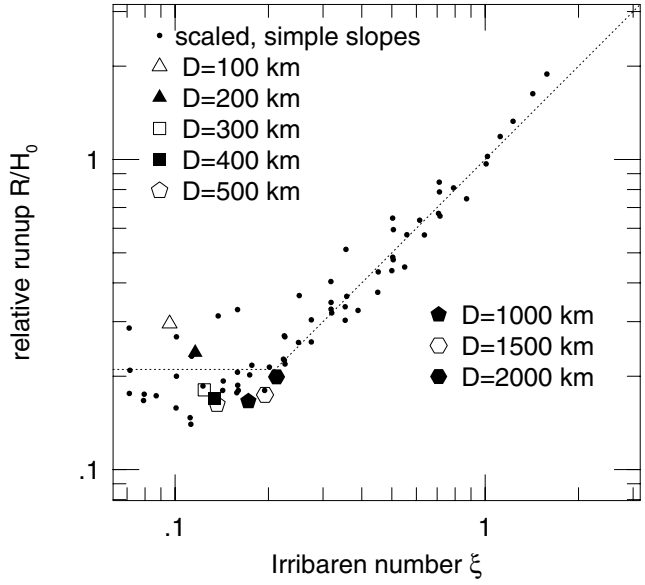

Figure 12. The relative run-up R/H_0 plotted versus Irribaren number $\xi = s(H_0/L_0)^{-1/2}$ for full-scale tsunami wave trains along with results for scaled wave trains propagating onto simple slopes as in Fig. 6. The dashed line is the piecewise linear fit $R/H_0 = \xi_0 (\xi < \xi_0)$, $R/H_0 = \xi$ $(\xi \geq \xi_0)$, for $\xi = 0.22$.

to be the average slope shore-wards of the breaking point. Given the scatter of the scaled-wave train results (as well as the other, simpler cases), it is difficult to be more precise about the extent of deviation from a presumably more clear-cut result. The fit to eq. (3) is $\xi_0 = 0.22$.

4 CONCLUSION

To help assess the hazard due to impact tsunami, we have applied the wave-propagation code COULWAVE to the calculation of the on-shore run-up of waves generated by the collapse of a cavity on the deep ocean, such as would be produced by the impact of a 300-m diameter object. Our primary interest is in determining the effects of non-linear processes, namely wave shoaling and breaking in the near shore region.

Large waves break at considerable distances off-shore, due to non-linear shoaling; this is the so-called 'Van Dorn effect' (Van Dorn *et al.* 1968; Le Méhauté 1971). Previous work of ours has confirmed its occurrence (Korycansky & Lynett 2005) and linked it to non-linear shoaling (Sakai & Battjes 1980). Non-linear shoaling (which is generally larger than linear-theory predictions by up to a factor of ∼2) may enhance wave dissipation, by causing waves to break much farther off-shore than one would otherwise expect.

Wave breaking has a considerable effect on the ultimate size of run-up. After breaking, wave lose energy due to the production of small-scale components that becomes turbulent and ultimately dissipate. COULWAVE incorporates a wave-breaking dissipation term that attempts to account for this and whose coefficients are calibrated by matching laboratory-scale experiments.

As noted above, we have found that the run-up R in this particular case—the impact of a 300-m diameter object off-shore of a generic North American depth profile—is between ∼18 and 30 per cent of the maximum waveheight $H_{\max}$ of the incident waves. For the closest impact ($D = 100$ km) $R \approx 0.3 H_{\max}$; the coefficient of proportionality decreases by about half for $D > 300$ km. Like the wave amplitude, R scales roughly as D^{-1}, where D is the distance from the impact site to the 800-m depth mark of the bathymetric profile, which is 40 km off-shore in our case.

Of more general usefulness is the comparison of relative run-up R/H_0 with the Irribaren number $\xi = s(H_0/L_0)^{-1/2}$. The run-up appears to follow the empirical relation suggested by Hunt (1959) and Battjes (1974), $R/H_0 = \xi$, for values of ξ greater than $\xi_0 \sim 0.1-0.2$. For smaller values of ξ, we find $R/H_0 \approx \xi_0$. While our results are scattered, they appear quite consistent over a wide range of wave heights, lengths and slopes. The regime $\xi < 0.2$ is both geophysically interesting from the point of view of impact-generated tsunami and more difficult to study. The wave steepness $w = H_0/L_0$, so that ξ can be written as $s w^{-1/2}$. Small values of ξ correspond to steep waves and/or shallow slopes, that experimental study becomes more challenging.

We have restricted the scope of our study to waves that are considerably shorter than the long waves experienced from earthquake tsunami. We would not expect Irribaren scaling to continue to hold for waves whose lengths can be up to hundreds of times as long as the water depth. For such waves, experimental study is difficult to realize and numerical study is appropriate. Lynett (2007) has carried out an extensive set of simulations of the approach and run-up of long waves onto beaches including off-shore obstacles. Obstacles generally act to reduce run-up, which is primarily affected by the beach slope; breaking waves like those discussed here, run up farthest on steep slopes, while for non-breaking waves, shallow slopes produce the largest run-up.

Assuming the validity of our result, it can be used as part of a scheme to assess hazards from tsunami, as has been done by Ward & Asphaug (2000) and Chesley & Ward (2006). The former study combined the relevant factors, such as cavity characteristics as functions of impactor parameters, rules for wave decay and (linear-theory) wave shoaling on a generic ocean profile, impactor ablation due to the atmosphere (which is important for stony asteroids of diameters less than 200 m), impactor rates, and statistical uncertainties to produce estimates of probabilities of impact tsunami exceeding specified heights over a specified time interval, for both generic sites and specific locations. Chesley & Ward (2006) used a simplified version of the physical factors and added population statistics near coasts to come up with estimates of economic losses and numbers of people affected by impact tsunami. Our work (both in this study and the results found by Korycansky & Lynett 2005) would modify these procedures in two ways. First, non-linear shoaling theory (e.g. Sakai & Battjes 1980) would identify locations x_b and depths h_b where waves would break, given the parameters H_0 and L_0 of the waves, which are functions of the impactor characteristics (principally the impactor diameter) and distance from the impact point. Then, given $s_b = h_b/x_b$, H_0, and L_0, the run-up would be calculated for the specific impact. The process could then be integrated over all impact points of interest (the deep ocean) and the impactor population to yield tsunami hazard estimates.

ACKNOWLEDGMENTS

We thank Steven Ward for supplying the input surface wave trains for the calculations described in Section 3, as well as a helpful review of the manuscript. Support for DGK was provided by NASA grant NNG04G851G 'Impact Tsunami: Ocean Wave Propagation'. Most of the calculations described in this paper were carried out on the UpsAnd beowulf computer cluster at UCSC funded by National Science Foundation MRI Grant AST-0079757. The paper has

been improved by the comments of Galen Gisler and an anonymous referee, for which we thank them.

REFERENCES

Atkinson, H., Tickell, C. & Williams, D., 2000. *Report of the UK Task Force on Potentially Hazardous NEOs*, available on-line at http:www.nearearthobjects.co.uk.

Baldock, T.E. & Holmes, P., 1999. Simulation and prediction of swash oscillations on a steep beach, *Coastal. Eng.,* **36,** 219–242.

Battjes, J.A., 1974. Surf similarity, *Proceedings of the 14th Coastal Eng. Conf.,* 466–479, Am. Soc. Civ. Eng., New York.

Bowen, A.J., Inman, D.L. & Simmons, V.P., 1968. Wave 'set-down' and set-up, *J. Geophys. Res.,* **73,** 2569–2577.

Bruun, P. & Günbak, A.R., 1977. Stability of sloping structures in relation to $\xi = \tan\alpha/\sqrt{H/L_0}$ risk criteria in design, *Coastal Eng.,* **1,** 287–322.

Cartwright, N., Nielsen, P. & Jessen, O.Z., 2002. Swash zone and near-shore water table dynamics, *Proceedings of the 28th Coastal Eng. Conf.,* 1006–1015, World Scientific, Singapore.

Chapman, C.R. & Morrison, D., 1994. Impacts on the Earth by comets and asteroids—assessing the hazard, *Nature,* **367,** 33–40.

Chawla, A. & Kirby, J.T., 2000. A source function method for generation of waves on currents in Boussinesq models, *Appl. Ocean Res.,* **22,** 75–83.

Chesley, S.R. & Ward, S.N., 2006. A quantitative assessment of the humanand economic hazard from impact-generated tsunami, *Nat. Hazards,* **38,** 355–374.

Cokelet, E.D., 1977. Steep gravity waves in water of arbitrary uniform depth, *Phil. Trans. R. Soc. London,* **286,** 183–230.

Dijabnia, M., 2002. Observations of waves in the surf and swash zones using particle image velocimetry, *Proceedings of the 28th Coastal Eng. Conf.,* 955–967, World Scientific, Singapore.

Dingemans, M., 1994. Comparison of computations with Boussinesq-like models and laboratory experiments, *Mast-G8M Note No. H1684*, Delft Hydraulics, Delft, The Netherlands.

Elfrink, B. & Baldock, T., 2002. Hydrodynamics and sediment transport inthe swash zone: a review and perspectives, *Coastal Eng.,* **45,** 149–167.

Gisler, G., Weaver, R., Gittings, M.L. & Mader, C., 2003. Two-and three-dimensional simulations of asteroid ocean impacts, *Sci. Tsunami Hazards,* **21,** 119–134.

Guza, R.T. & Thornton, E.B., 1981. Wave set-up on a natural beach, *J. Geophys. Res.,* **85,** 1524–1530.

Guza, R.T. & Thornton, E.B., 1982. Swash oscillations on a natural beach, *J. Geophys. Res.,* **86,** 4133–4137.

Gourlay, M.R., 1992. Wave set-up, wave run-up, and beach water table: interaction between surf zone hydraulics and groundwater hydraulics, *Coastal Eng.,* **17,** 93–144.

Hansen, J.B. & Svendsen, I.A., 1979. Regular waves in shoaling water, experimental data, Series Paper 21, ISVA. Techn. Univ. Denmark.

Hanslow, D. & Nielsen, P., 1993. Shoreline set-up on natural beaches, *J. Coastal Res.,* **15,** 1–10.

Hills, J.G., Nemchinov, I.V., Popov, S.P. & Teterev, A.V., 1994. Tsunami generated by small asteroid impacts, in *Hazards Due to Comets and Asteroids*, pp. 779–789, ed. Gehrels, T., Arizona Press, Tucson.

Holman, R.A., 1986. Extreme value statistics for wave run-up on a natural beach, *Coastal Eng.,* **9,** 527–544.

Holman, R.A. & Bowen, A.J., 1984. Longshore structure of infragravity wave motions, *J. Geophys. Res.,* **89,** 6446–6452.

Holman, R.A. & Guza, R.T., 1984. Measuring run-up on a natural beach, *Coast. Eng.,* **8,** 129–140.

Holman, R.A. & Sallenger A.H., Jr, 1985. Setup and swash on a natural beach, *J. Geophys. Res.,* **90,** 945–953.

Howd, P.A., Oltman-Shay, J. & Holman, R.A., 1991. Wave variance partitioning in the trough of a barred beach, *J. Geophys. Res.,* **96,** 12 781–12 795.

Hunt, L.A., 1959. Design of seawalls and breakwaters, *Proc. Am. Soc.Civ. Eng., J. Waterways and Harbors Div.,* **85,** WW3.

Jordaan, J.M., 1972. Impulsive waves: model and prototype correlations. in *Advances in Hydroscience*,Vol. 8, pp. 261–304, ed. Chow, V.T., Academic Press, New York.

Kennedy, A.B., Chen, Q., Kirby, J.T. & Dalrymple, R.A., 2000. Boussinesqmodel of wave transformation, breaking, and run-up. Part I: 1D, *J. Waterway Port Coast Ocean Eng.,* **126,** 39–47.

Kirby, J.T., 1997. Nonlinear, dispersive long waves in water of variable depth, in *Advances in Fluid Dynamics*,Vol. 10, pp. 550–125, ed. Hunt, J.N., Computational Mechanics Publications, Southampton.

Korycansky, D.G. & Lynett P.J., 2005, Offshore breaking of impact tsunami: the Van Dorn effect re-visited, *Geophys. Res. Lett.,* **32,** L10805.

Le Méhauté, B., 1971. Theory of explosion-generated water waves, in *Advances in Hydroscience*,Vol. 7, pp. 1–74, ed. Chow, V.T., Academic Press, New York.

Le Méhauté, B. & Wang, S., 1996. *Water Waves Generated by Underwater Explosion*, 357 pp., World Scientific, Singapore.

Liu, P.L.-F., 1994. Model equations for wave propagation from deep to shallow water, in *Advances in Coastal and Ocean Engineering,*Vol. 1, pp. 125–157, ed. Liu, P.L.-F., World Scientific, Singapore.

Lynett, P.J., 2006. Nearshore wave modeling with high-order Boussinesq-type equations, *J. Waterway Port Coastal Eng.,* **132,** 348–357.

Lynett, P.J., 2007. The effect of a shallow water obstruction on long wave run-up and overland flow velocity, *J. Waterway Port Coastal Eng.,* in press.

Lynett, P.J., Wu, T.-R. & Liu, P.L.-F., 2002. Modeling wave run-up with depth-integrated equations, *Coastal Eng.,* **46,** 89–107.

Mader, C.L. & Gittings, M.L., 2002. Modeling the 1958 Lituya Bay Megatsunami, II. *Sci. Tsunami Hazards,* **20,** 241–250.

Miller, D.J., 1960. Giant waves in Lituya Bay. *Geo. Soc. America Professional Paper #354,* at https://www.uwsp.edu/geo/projects/geoweb/participants/dutch/ LituyaBay/Lituya0.HTM

Miller, D.J., 1960. The Alaska earthquake of July 10, 1958: giant wave in Lituya Bay, *Bull. seism. Soc. Amer.,* **50,** 253–266.

Morang, A. & Garcia, A., eds, 2002. *Coastal Engineering Manual,* The US Army Engineer Research and Development Centers Coastal &Hydraulics Laboratory.

Melosh, H.J., 1989. *Impact Cratering*, Oxford University Press, New York.

Melosh, H.J., 2003. Impact-generated tsunamis: an over-rated hazard, *34th Lun. Plan. Sci. Conf.,* #2013. (Abstract).

Nielsen, P. & Hanslow, D.J., 1991. Wave run-up distributions on natural beaches, *J. Coastal Res.,* **7,** 1139–1152.

Nwogu, O., 1993. Alternative form of Boussinesq equations for nearshore wave propagation, *J. Waterway Port Coast Ocean Eng.,* **119,** 618–638.

Raubenheimer, B., 2002. Observations and predictions of fluid velocities in the surf and swash zones, *J. Geophys. Res.,* **107,** 3190.

Raubenheimer, B. & Guza, R.T., 1996. Observations and predictions of run-up, *J. Geophys. Res.,* **101,** 25 575–25 587.

Raubenheimer, B., Guza, B.T., Elgar, S. & Kobayashi, N., 1995. Swash on a gently sloping beach, *J. Geophys. Res.,* **100,** 8751–760.

Raubenheimer, B., Guza, B.T. & Elgar, S., 2001. Field observations of wave-driven setdown and setup, *J. Geophys. Res.,* **106,** 4629–4638.

Roos, A. & Battjes, J.A., 1976. Characteristics of flow in run-up of periodic waves, *Proc. 15th Coastal Eng. Conf.,* 781–795.

Ruessink, B.K., Kleinhans, M.G. & van den Beukel, P.G.L., 1998. Observations of swash under highly dissipative conditions, *J. Geophys. Res.,* **103,** 3111–3118.

Ruggiero, P., Komar, P.D., McDougal, W.G., Marra, J.J. & Beach, R.A., 2001. Wave run-up, extreme water levels and the erosion of properties backing beaches, *J. Coastal Res.,* **17,** 407–419.

Ruggiero, P., Holman, R.A. & Beach, R.A., 2004. Wave run-up on a high-energy dissipative beach, *J. Geophys. Res.,* **109,** C06 025.

Sakai, T. & Battjes, J.A., 1980. Wave shoaling calculated from Cokelet's theory, *Coastal Eng.,* **4,** 65–84.

Schmidt, R.M. & Housen, K.R., 1987. Some recent advances in the scaling of impact and explosive cratering, *Int. J. Impact Eng.,* **5,** 543–560.

Stockdon, H.F., Holman, R.A., Howd, P.A. & Sallenger, A.H., 2006. Empirical parameterization of setup, swash, and run-up, *Coastal Eng.,* **53,** 573–588.

Ting, F.C.-K. & Kirby, J.T., 1995. Dynamics of surf-zones turbulence in a strong plunging breaker, *Coastal Eng.,* **24,** 177–204.
Ting, F.C.-K. & Kirby, J.T., 1996. Dynamics of surf-zones turbulence in a spilling breaker, *Coastal Eng.,* **26,** 131–160.
Titov, V.V. & Synolakis, C.E., 1995. Modeling of breaking and nonbreaking long-wave evolution and run-up using VTCS-2, *J. Waterways, Ports, Ocean Eng.,* **121,** 308–316.
Van Dorn, W.G., 1961. Some characteristics of surface gravity waves in the sea produced by nuclear explosions, *J. Geophys. Res.,* **66,** 3845–3862.
Van Dorn, W.G., 1976. Set-up and run-up in shoaling breakers, *Proc. 15th Coastal Eng. Conf.,* 738–751, Am. Soc. Civ. Eng., New York.
Van Dorn, W.G., 1978. Breaking invariants in shoaling waves, *J. Geophys. Res.,* **83,** 2981–2988.
Van Dorn, W.G., Le Méhauté, B. & Hwang, L.-S., 1968. Handbook of explosion-generated water waves. Tetra Tech Inc.
Ward, S.N. & Asphaug, E., 2000. Asteroid impact tsunami: a probabilistic hazard assessment, *Icarus,* **145,** 64–78.
Ward, S.N. & Asphaug, E., 2003. Asteroid impact tsunami of 2880 March 16, *Geophys. J. Int.,* **153,** F6–F10.
Ward, S.N. & Day, S., 2003. Ritter Island Volcano - lateral collapse and the tsunami of 1888. *Geophys. J. Int.,* **155,** 891–902.
Wei, G., Kirby, J.T., Grilli, S. & Subramanya, R., 1995. A fully nonlinear Boussinesq model for surface waves. Part I: highly nonlinear unsteady waves, *J. Fluid Mech.,* **294,** 71–92.
Weiss, R., Wünnemann, K. & Bahlburg, H., 2006. Numerical modelling of generation, propagation, and run-up of tsunamis caused by ocean impacts: model strategy and technical solutions, *Geophys. J. Int.,* **67,** 77–88.
Wright, L.D. & Short, A.D., 1984. Morphodynamic variability of surf zones and beaches: a synthesis, *Marine Geol.,* **56,** 93–118.

APPENDIX A: MODEL EQUATIONS

The model equations we solve are essentially the same as given by (Lynett *et al.* 2002):

$$\frac{\partial \zeta}{\partial t} + E = E_s, \qquad \frac{\partial u}{\partial t} + F - R_f - R_b - R_v = 0. \tag{A1}$$

The basic variables are the surface height ζ and the fluid (particle) velocity u referred to the reference water depth $z_\alpha = -0.531h$, where h is the local (undisturbed) water depth. The value of z_α is chosen to optimize agreement between the equations and linear dispersion relation for depth-resolved waves (Nwogu 1993). The surface driver term E_s has been described in the main text. The terms E and F derive from expansions of the full 2-D equations in powers of $\epsilon = a/h$ and kh, where a is the typical wave amplitude, h is the depth, and $k = 2\pi/L$ is the wavenumber for a wave of length L. E and F are given by

$$E = \frac{\partial}{\partial x}[(h+\zeta)u] - \frac{\partial}{\partial x}\left\{\left[\left(\frac{1}{6}(\zeta^2 - \zeta h + h^2) - \frac{z_\alpha^2}{2}\right)\frac{\partial^2 u}{\partial x^2} + \left[\frac{1}{2}(\zeta - h) - z_\alpha\right]\frac{\partial^2 (hu)}{\partial x^2}\right]\right\} \tag{A2}$$

and

$$\begin{aligned} F = {} & u\frac{\partial u}{\partial x} + g\frac{\partial \zeta}{\partial x} + \frac{1}{2}z_\alpha^2\frac{\partial^3 u}{\partial x^2 \partial t} + z_\alpha\frac{\partial^2}{\partial x^2}\left(h\frac{\partial u}{\partial t}\right) + \left(\frac{\partial}{\partial x}(hu) + u\frac{\partial z_\alpha}{\partial x}\right)\frac{\partial^2}{\partial x^2}(hu) \\ & - \frac{\partial}{\partial x}\left(\zeta\frac{\partial^2}{\partial x \partial t}(hu)\right) + z_\alpha\frac{\partial}{\partial x}\left(u\frac{\partial^2}{\partial x^2}(hu)\right) + z_\alpha u\frac{\partial z_\alpha}{\partial x}\frac{\partial^2 u}{\partial x^2} + \frac{z_\alpha^2}{2}\frac{\partial}{\partial x}\left(u\frac{\partial^2 u}{\partial x^2}\right) \\ & + \frac{\partial}{\partial x}\left[-\frac{\zeta^2}{2}\frac{\partial^2 u}{\partial x \partial t} - \zeta u\frac{\partial^2}{\partial x^2}(hu) - \zeta\frac{\partial u}{\partial x}\frac{\partial}{\partial x}(hu)\right] + \frac{\partial}{\partial x}\left\{\frac{\zeta^2}{2}\left[\left(\frac{\partial u}{\partial x}\right)^2 - u\frac{\partial^2 u}{\partial x^2}\right]\right\}. \end{aligned} \tag{A3}$$

The partial upwinding mentioned in the text was applied to the advective term $u\partial u/\partial x$ in eq. (A3). More numerical details (such as the differencing scheme and the treatment of the shoreline boundary) are given by Lynett *et al.* (2002). The terms R_f and R_b, account for bottom drag and wave breaking. Bottom friction is modelled by a quadratic term:

$$R_f = \frac{f}{h+\zeta}u|u|, \tag{A4}$$

and wave breaking is modelled using the formulation developed by Kennedy *et al.* (2000) [also described by Lynett (2006)]:

$$R_b = \frac{1}{h+\zeta}\frac{\partial}{\partial x}\left[\nu_b\frac{\partial}{\partial x}[(h+\zeta)u]\right], \tag{A5}$$

where ν_b is a time- and space-dependent coefficient. The breaking model is turned on (i.e. $\nu_b > 0$) at a gridpoint x when the local time derivative $\partial\zeta/\partial t$ exceeds a critical value $(\partial\zeta/\partial t)^I$. When this criterion is not met $\nu_b = 0$ and no damping is applied. The time when breaking is turned on is denoted by t_0; damping is applied for $t > t_0$ as long as $\partial\zeta/\partial t > (\partial\zeta/\partial t)^*$, the latter criterion being a function of time. The coefficient ν_b is given by

$$\nu_b = B\delta^2(h+\zeta)\frac{\partial \zeta}{\partial t}, \tag{A6}$$

where (subscript t denoting time derivatives)

$$B = \begin{cases} 0, & \zeta_t \le \zeta_t^*, \\ \zeta_t/\zeta_t^* - 1 & \zeta_t^* < \zeta_t \le 2\zeta_t^*, \\ 1, & \zeta_t > 2\zeta_t^*, \end{cases} \qquad \zeta_t^* = \begin{cases} \zeta_t^I + \frac{t-t_0}{T^*}(\zeta_t^F - \zeta_t^I), & 0 \le t - t_0 < T^*, \\ \zeta_t^F, & t - t_0 > T^*. \end{cases} \tag{A7}$$

The coefficients were set by matching experimental results (Hansen & Svendsen 1979) to

$$\delta = 6.5,\ T^* = 7[(h+\zeta)/g]^{1/2},\ \zeta_t^I = 0.65[g(h+\zeta)]^{1/2},\ \text{and}\ \zeta_t^F = 0.08[g(h+\zeta)]^{1/2}. \tag{A8}$$

Additional numerical viscosity is provided by the term R_ν as described in the text:

$$R_\nu = \nu\left\{ -\frac{\partial^2}{\partial x^2}\left[\frac{z_\alpha^2}{2}\frac{\partial^2 u}{\partial x^2} + z_\alpha\frac{\partial (hu)}{\partial x^2}\right] + \frac{\partial}{\partial x}\left[\frac{\zeta^2}{2}\frac{\partial^3 u}{\partial x^3} + \zeta\frac{\partial^3 (hu)}{\partial x^3}\right]\right\}, \tag{A9}$$

where as noted above $\nu = \nu_0(gh_0^3)^{1/2}$, with $\nu_0 = 10^{-5}$, and h_0 is the depth at the boundary where the waves are generated.